

Special Issue

Solar Cells Utilizing Small Molecular Weight Organic Semiconductors

Barry P. Rand*[†], Jan Genoe, Paul Heremans and Jef Poortmans

Polymer and Molecular Electronics, IMEC, Kapeldreef 75, B-3001 Leuven, Belgium

In this review, we focus on the field of organic photovoltaic cells based on small molecular weight materials. In particular, we discuss the physical processes that lead to photocurrent generation in organic solar cells, as well as the various architectures employed to optimize device performance. These include the donor–acceptor heterojunction for efficient exciton dissociation, the exciton blocking layer, the mixed or bulk heterojunction, and the stacked or tandem cell. We show how the choice of materials with known energy levels and absorption spectra affect device performance, particularly the open-circuit voltage and short-circuit current density. We also discuss the typical materials and growth techniques used to fabricate devices, as well as the issue of device stability, all of which are critical for the commercialization of low-cost and high-performance organic solar cells. Copyright © 2007 John Wiley & Sons, Ltd.

KEY WORDS: organic solar cells; donor acceptor interface; exciton dissociation; stacked cell; bulk heterojunction; exciton blocking layer

Received 29 May 2007; Revised 25 July 2007

INTRODUCTION

The field of organic electronics^{1–3} is rapidly maturing into one where new applications and products are currently in development. The main reason for the widespread interest in organic semiconducting materials is their potential for low cost, ease of processing, and compatibility with flexible substrates. Among the most promising electronic and photonic devices that make up the organic electronics' collection are organic light emitting diodes,^{4–6} organic transistors,^{7,8} and organic photovoltaic (PV) cells.^{9–11}

Within the research area of organic-based PV cells, there are multiple approaches which are all being actively pursued. These various approaches include the dye-sensitized solar cell (DSSC),^{12,13} organic/inorganic hybrid cells,^{14,15} and organic PV

cells based on a heterojunction (HJ) between polymeric^{16–18} or small molecular weight organic materials.^{19,20} Of these, the solid-state DSSC, polymer, and small molecular weight based devices have all achieved efficiencies of between 4 and 5% for a single cell.^{13,21–23} Keeping pace with this rapid increase in device efficiency is the number of refereed journal publications related to organic PV materials and devices,²⁴ which has increased exponentially for approximately the past three decades, as shown in Figure 1. Here, we focus our attention on the physics and operation of thin film PV cells based upon HJs of small molecular weight organic semiconductors.

The design of organic PV cells needs to be inherently different from architectures employed for inorganic cells.²⁵ This is specifically due to the differences in physical properties between organic and inorganic semiconductors. For example, photon absorption in an organic semiconductor results in the creation of an exciton, or bound electron–hole pair,

*Correspondence to: Barry P. Rand, Polymer and Molecular Electronics, IMEC, Kapeldreef 75, B-3001 Leuven, Belgium.

[†]E-mail: Barry.Rand@imec.be

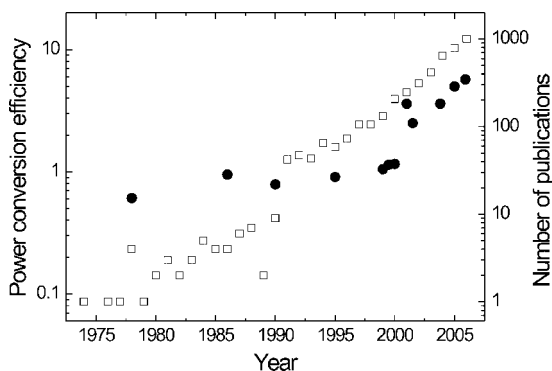


Figure 1. Timeline of the power conversion efficiency of small molecule-based organic photovoltaic cells (filled circles) and the number of journal publications related to organic-based photovoltaics (open squares)

as opposed to the creation of free charge carriers which would result from photon absorption in an inorganic solid. Contributing to this property are the weak, non-covalent, van der Waals interactions between molecules; this results in a low intermolecular orbital overlap and low dielectric constant for the solid. Furthermore, organic semiconductors tend to have rather low charge carrier mobilities (typically 10^{-5} – $0.1 \text{ cm}^2/\text{Vs}$) as well as small exciton diffusion lengths ($L_D \approx 3$ – 40 nm). However, most organic materials possess high absorption coefficients of $\alpha > 10^5 \text{ cm}^{-1}$,²⁰ which means that layer thicknesses can be kept thin yet still highly absorptive while simultaneously preserving good charge transport. The understanding of these parameters forms the rationale for the various device architectures presented here, and is the reason for the rapid progress in the field recently.

This review is organized as follows: following a brief tutorial of the PV device principle, we present the necessary theory for the understanding of organic photocurrent generation as well as open-circuit voltage in organic PV cells in Section “Theory”. An overview of common materials as well as growth techniques used to fabricate devices is provided in Section “Typical Materials and Growth Techniques”. Section “Device Architectures” is devoted to explaining the various device architectures that have been developed to increase the performance of organic PV cells. The issue of device lifetime is discussed in Section “Device Stability”. Finally, we conclude and offer our perspective on the challenges to achieving higher efficiencies in Section “Conclusions”.

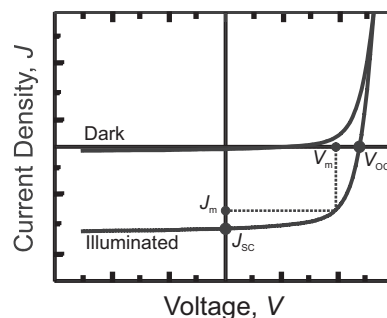


Figure 2. Typical current density vs. voltage (J – V) curves of a solar cell in the dark and under illumination. The various device parameters are also shown, including open-circuit voltage (V_{OC}), short-circuit current density (J_{SC}), and the points of current and voltage (J_m and V_m , respectively) that correspond to maximum power output. The rectangular region in the fourth quadrant indicates maximum power output

THEORY

Photovoltaic fundamentals

Power generation by a PV cell is a process to convert light energy into electrical energy.²⁶ The light incident on the cell results in a separation of charge carriers, which ultimately gives rise to photocurrent that does work on an external load. This section discusses how PV cells work, and how to calculate their power efficiency.

Current density–voltage (J – V) characteristics for a typical PV cell in the dark and under incident illumination are shown in Figure 2. The figure also shows the short-circuit current density, J_{SC} , and open-circuit voltage, V_{OC} , under illumination. The operating range of the solar cell is therefore $0 < V < V_{OC}$, where the device generates power. The fill factor (FF) is calculated as

$$\text{FF} = \frac{J_m V_m}{J_{SC} V_{OC}} \quad (1)$$

where the product $J_m V_m$ corresponds to the maximum power point. Then, the power conversion efficiency, η_P , is

$$\eta_P = \frac{J_m V_m}{P_0} = \frac{J_{SC} V_{OC} \text{FF}}{P_0} \quad (2)$$

where P_0 is the incident light intensity.

The equivalent circuit of an organic PV cell is shown in Figure 3, and forms the basis for its J – V characteristics. The photocurrent source, J_{ph} ,

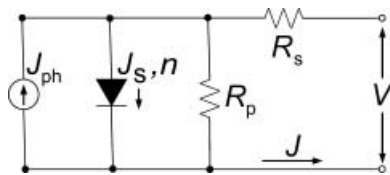


Figure 3. Equivalent circuit for an organic photovoltaic cell. The series and parallel resistances are R_s and R_p , respectively, n is the diode ideality factor, and J_S and J_{ph} are the reverse saturation and photocurrent densities, respectively

opposes the dark current of the diode, J_{dark} . The J - V characteristics can then be expressed by the generalized Shockley equation:²⁷

$$J = \frac{R_p}{R_s + R_p} \left[J_S \left\{ \exp \left(\frac{q(V - JR_s)}{nk_B T} \right) - 1 \right\} + \frac{V}{R_p} - J_{ph}(V) \right] \quad (3)$$

where R_s and R_p are the series and parallel resistances, respectively, n is the diode ideality factor, q is the electron charge, k_B is Boltzmann's constant, T is temperature, and J_S is the reverse saturation current density. The dark current density is also given by Equation (3) when $J_{ph} = 0$.

The generalized Shockley equation (Equation (3)) describes the J - V characteristics of a non-ideal diode, and thus most organic PV cells. In an ideal diode and solar cell, $R_s = 0$, $R_p = \infty$, $n = 1$, and $J_{ph} \neq J_{ph}(V)$. Apart from non-zero R_s and finite R_p , some common deviations from an ideal diode observed for organic heterojunctions are the following: R_p dependent on light intensity²⁸⁻³⁰ as $R_p \propto P_0^{-1}$, R_s sometimes decreases with increased light intensity causing a crossing of the light and dark curves at positive current densities,³¹ $n > 2$, a "kink" in the J - V curve near open-circuit,³¹⁻³³ and a voltage-dependent photocurrent.^{28,29,32} The inverse and linear dependence of R_p on P_0 suggests an increase in free charge carriers in the bulk produced either as a result of exciton annihilation transferring energy to trapped charges,^{28,34} or from photoconductive gain, as these processes are dependent on exciton density which is directly proportional to P_0 . The reduced R_s which has been observed under light illumination likely comes from photoconductive gain in the organic film which decreases the resistance to carrier flow through the bulk film. The "kink" which has been reported near open-circuit remains a topic of continued

research, but could be due to poor carrier extraction at the contacts³³ or to poor charge transfer at the donor/acceptor interface,^{31,32} resulting in a voltage-dependent photocurrent, a topic which will be discussed in Subsection "Photocurrent."

These non-idealities have important consequences for device performance, for example on FF, which will be affected as²⁷

$$FF(R_s, R_p) \approx FF(0, \infty) \left(1 - \frac{J_{SC} R_s}{V_{OC}} - \frac{V_{OC}}{J_{SC} R_p} \right) \quad (4)$$

Equation (4) indicates that FF is reduced below its maximum in junctions with high R_s and low R_p . Thus, efforts to reduce R_s in organic solar cells should be taken to ensure a high FF.³⁵ Also, it should be stressed that the reduction of R_p with P_0 , a general characteristic of organic solar cells, ultimately reduces FF and therefore η_P at high light intensities.

The donor/acceptor heterojunction concept

The field of organic photovoltaics started with single layers of an organic semiconductor, deposited between electrodes made up of two different metals, to produce a rectifying device. These devices produced rather low efficiencies of $\eta_P \approx 0.01\%$.³⁶ These numbers improved dramatically when Tang introduced a thin film organic PV cell composed of a donor-acceptor (DA) HJ in 1986, with $\eta_P = 0.95\%$.³⁷ The DA interface allows for efficient dissociation of excitons in comparison to that possible in a single organic layer, as will be discussed below. In fact, in the years following this seminal work, the number of publications increased sharply (see Figure 1), indicating the importance of this advancement.

A schematic energy diagram of the DA HJ, consisting of a donor- and an acceptor-type molecular layer, is shown in Figure 4. In this diagram, the donor material has both a lower highest occupied molecular orbital (HOMO), or ionization potential (IP), and lowest unoccupied molecular orbital (LUMO), or electron affinity (EA), than that of the acceptor layer. For an organic semiconductor, the difference between the IP and EA is known as the transport gap, E_{tran} . The optical energy gap of each material, E_{opt} , is taken as the point of the low-energy absorption edge. The exciton binding energy, $E_B = IP - EA - E_{opt}$, typically varies from 0.2 eV to 1 eV for organic semiconductors.^{38,39}

Proper alignment of energy levels between the D and A layers allows for very efficient dissociation

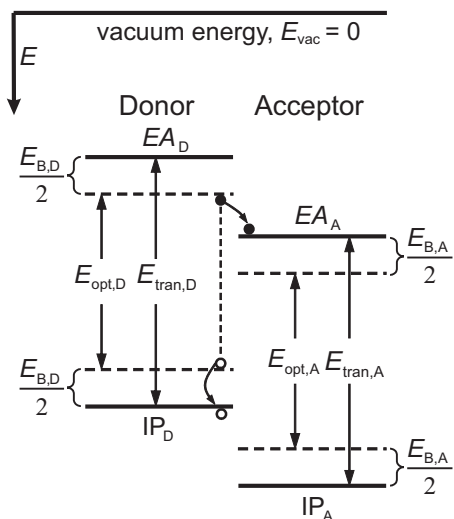


Figure 4. Schematic energy level diagram of an organic heterojunction between a donor (D) and an acceptor (A) layer. Here IP (or highest occupied molecular orbital (HOMO)) and EA (or lowest unoccupied molecular orbital (LUMO)) are the ionization potential and electron affinity, respectively. The exciton binding energy (E_B) of each material is equal to the difference between the transport gap (E_{tran}) and optical gap (E_{opt}). The vacuum energy (E_{vac}) is shown and is the point of zero energy, with the y -axis defined as the energy axis. The process of charge transfer of an exciton from $D \rightarrow A$ is also illustrated

of excitons at the DA interface⁴⁰ into a geminate pair, or Coulombically bound hole polaron in the donor material and electron polaron in the acceptor material, schematically illustrated for a donor exciton in Figure 4. The conditions for exciton dissociation to be energetically favorable are

$$E_{B,D} < EA_A - EA_D \quad (5a)$$

$$E_{B,A} < IP_A - IP_D \quad (5b)$$

where Equation (5a) considers a charge transfer reaction of a donor exciton ($D \rightarrow A$) and Equation (5b) is for charge transfer of an acceptor exciton ($A \rightarrow D$). This process is intrinsically more efficient than dissociation of excitons in the bulk of an organic material, which can be estimated by using an Onsager model for charge-pair dissociation,⁴¹ and requires applied fields in excess of 10^6 V/cm to overcome the pair binding energy and have an appreciable dissociation probability.⁴² Fields with this strength are not generated at the low forward biases at which PV

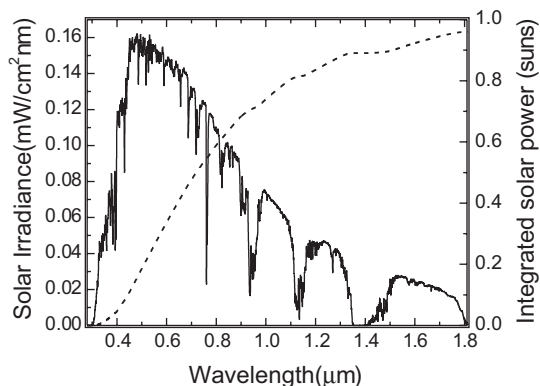


Figure 5. The spectral irradiance (solid line) for air mass 1.5 global solar radiation. When integrated over the full solar spectrum, the area is equal to 1 sun (100 mW/cm^2) intensity. The dashed line shows the integrated solar power vs. wavelength

cells operate, therefore explaining the observed low efficiencies of single layer devices.

Photocurrent

The standard testing conditions for a solar cell are $P_0 = 100 \text{ mW/cm}^2$ under air mass 1.5 global illumination (1 sun, AM1.5G, shown in Figure 5), and 298 K. In fact, care should be taken by following standardized testing criteria to ensure reporting correct efficiency values.^{43,44} The photocurrent density of the cell is given as

$$J_{ph}(V) = \int \frac{q\lambda}{hc} \eta_{EQE}(\lambda, V) S(\lambda) d\lambda \quad (6)$$

where λ is the wavelength, h is Planck's constant, c is the speed of light, $S(\lambda)$ is the spectral irradiance of the incident light, and η_{EQE} is the external quantum efficiency of the device, or the number of charge carriers collected at the electrodes with respect to the number of photons incident on the device. Note that $J_{ph}(0) = J_{SC}$.

For a DA interface, η_{EQE} can be described via a four-step process, defined as

$$\eta_{EQE}(\lambda, V) = \eta_A(\lambda) \eta_{ED} \eta_{CT}(V) \eta_{CC}(V) \quad (7)$$

Here, η_A , the first process, is the absorption efficiency of the various layers in the device. The next step is that of exciton diffusion, where η_{ED} gives the percentage of photogenerated excitons that diffuse to a DA interface.

Excitons that reach a DA HJ undergo a charge transfer step with an efficiency η_{CT} to dissociate into holes in the donor and electrons in the acceptor layers. Finally, η_{CC} is the charge collection efficiency, or the fraction of dissociated excitons that are collected at the electrodes.

The processes of absorption and exciton diffusion can be accurately modeled following a technique which has previously been established by Petterson *et al.*⁴⁵ In this transfer-matrix based approach, the dielectric constants and thicknesses of each layer in the solar cell are used to determine η_A , and give an optical field intensity distribution within the active layers as a function of both wavelength and position. From this, one can calculate the generation rate of excitons within the active layers that takes optical interference effects into account. Then, by solving the diffusion equation with known L_D for the D and A materials, η_{ED} is determined. As a consequence, the photocurrent of an organic PV cell is proportional to L_D , and it is therefore beneficial to find or design molecules to optimize this parameter.⁴⁶ The exciton diffusion lengths for various materials can be determined either by measurement via photoluminescence quenching experiments,⁴⁷ or by fitting the experimental $\eta_{EQE}(\lambda)$ to the results of the model in the case of a material which is non-emissive.²⁰ It is important to note that optical modeling of these thin film structures is crucial for the proper design of layer thicknesses, due to optical interference in the very thin films (often ~ 10 – 40 nm) used in these devices.

The charge transfer efficiency becomes appreciable when the conditions of Equation (5) are satisfied. To more accurately calculate η_{CT} , the Marcus theory for electron transfer,⁴⁹ schematically illustrated in Figure 6, and which describes the transfer rate as a function of the frontier energy level (LUMO/LUMO or HOMO/HOMO) offset, can be applied. In fact, this theory has been used for the case of molecular-based photovoltaic cells,^{28,31,48,50,51} and in particular to describe the dependence of $\eta_{CT}(V)$ ^{28,31,48} as the ratio of the forward and reverse transfer rates. The electron transfer rate, k_{if} , where i and f represent initial and final energy levels, is given as

$$k_{if} = \left(\frac{4\pi^3}{\hbar^2 \lambda_{if} k_B T} \right)^{1/2} V_{if}^2 \exp \left(- \frac{(E_{if} + \lambda_{if})^2}{4\lambda_{if} k_B T} \right) \quad (8)$$

Here, V_{if} is the electronic coupling matrix element, λ_{if} is the molecular reorganization energy, and

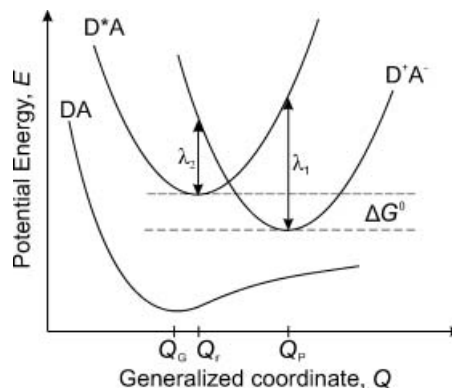


Figure 6. Potential energy curves and charge transfer between a donor/acceptor pair. The ground state (DA), lowest intramolecular donor excited state (D*A), and the lowest charge-transfer state (D+A⁻) are all illustrated. Also shown are the electron affinity offset between the donor and acceptor (ΔG^0) and the reorganization energy, λ . Adapted from Reference [48]

$E_{if} = E_i - E_f$ is the free energy difference (ΔG^0 in Figure 6) between frontier energy levels i and f (for exothermic transfer, $E_{if} < 0$). This equation neglects tunneling contributions which may aid in charge transfer, and result in more reasonable values of V_{if} . For a discussion, see Reference [48]. An interesting consequence of Marcus theory is that k_{if} between the donor and acceptor initially increases with E_{if} . However, as E_{if} becomes greater than λ_{if} , k_{if} ultimately decreases. This is known as the inverted region, and has important consequences for the design of organic PV cells, in that one needs to find materials with energy levels to optimize the forward transfer rate, but without entering the inverted region which would in fact reduce η_{CT} and therefore J_{SC} . Furthermore, as E_{if} is tuned to increase k_{if} , the device V_{OC} changes, as will be explained in Subsection “Open-circuit voltage.”

The final contribution to η_{EQE} is that of η_{CC} , which is sensitively dependent on the nanomorphology of the DA structure. For example, a device composed of neat thin films of D and A can have $\eta_{CC} \approx 100\%$.²⁰ However, for a device with a bulk or mixed HJ, where trapping and recombination of the photogenerated charges are more likely, the resulting $\eta_{CC} < 1$, and decreases further with mixed layer thickness. This topic will be discussed in more detail in Subsection “Donor/acceptor interface” along with device architectures designed to avoid this complication.

Open-circuit voltage

Increasing the device V_{OC} has been the subject of significant research efforts^{52–55} owing to the fact that state of the art small molecule based PV cells have $V_{OC} \approx 0.5$ V, whereas the peak absorption of the constituent organic materials is at photon energies ≥ 2.0 eV. Therefore, this step generates a significant loss for organic PV cells, considering that in the case where qV_{OC} approaches the absorbed photon energy, efficiencies would be up to four times higher.

By solving Equation (3) at $J = 0$ for $V = V_{OC}$, we can highlight the factors that contribute to V_{OC} :

$$V_{OC} = \frac{nk_B T}{q} \ln \left[\frac{J_{ph}(V_{OC})}{J_S} + 1 - \frac{V_{OC}}{J_S R_p} \right] \quad (9)$$

Assuming η_{EQE} is not a function of the incident light intensity and the product $J_S R_p \gg V_{OC}$, then $V_{OC} \propto \ln(P_0)$. These conditions are normally satisfied at P_0 less than a few suns intensity.

There is significant experimental evidence to suggest that V_{OC} originates from the difference between the HOMO of the donor material and LUMO of the acceptor,^{28,56–61} as opposed to the work function differences between the metal electrodes. Ultimately, the maximum value of V_{OC} , V_{OC}^{max} , corresponds to²⁸

$$qV_{OC}^{max} = IP_D - EA_A - \frac{q^2}{4\pi\epsilon_0\epsilon_r r_{DA}} \quad (10)$$

where ϵ_0 is the vacuum permittivity, ϵ_r is the relative dielectric constant of the bulk organic layer, and r_{DA} is the initial separation distance of the electron–hole pair in the donor and acceptor layers immediately following charge transfer, and which needs to be fully separated to contribute to photocurrent.⁶² The third term on the right-hand side of Equation (10) is the binding energy of the dissociated, geminate electron–hole pair created as a result of electron transfer.

TYPICAL MATERIALS AND GROWTH TECHNIQUES

The performance of a molecular PV cell is dependent on three main factors: material selection, material growth technique, and device architecture. As a result of these choices, there is a nearly infinite number of possibilities in overall device selection. In this and the next section, we will attempt to review the most

common materials and growth techniques, as well as the various architectures that may be employed to optimize device performance.

Materials

The different classes of materials that form a complete device structure are the substrate, transparent conducting electrode, organic layers, and also a reflective metallic electrode. Exceptions to this will be discussed in Subsection “Other architectures.” The substrate is composed of either glass or, in some cases, a transparent flexible polymer foil.^{16,63–66} Then for the transparent electrode (typically the anode), the most common is that of indium-tin-oxide (ITO), but some alternatives are being developed in order to avoid using this costly material, for example other transparent conducting oxides,^{67,68} conducting polymers such as poly(3,4-ethylenedioxythiophene):poly(styrenesulfonate) (PEDOT:PSS),^{63,64,69} as well as composites of a conducting polymer with carbon nanotubes.^{70–74} The use of self-assembled monolayers on the ITO surface has also been investigated and has resulted in increased J_{SC} and decreased R_s .^{75,76} It remains to be seen if this same technique can be applied successfully to other anode surfaces. The other electrode (typically the cathode) is often a thick, reflective metal such as Al or Ag.

Figure 7 shows the structures of some molecules which are common to organic PV cell design. The

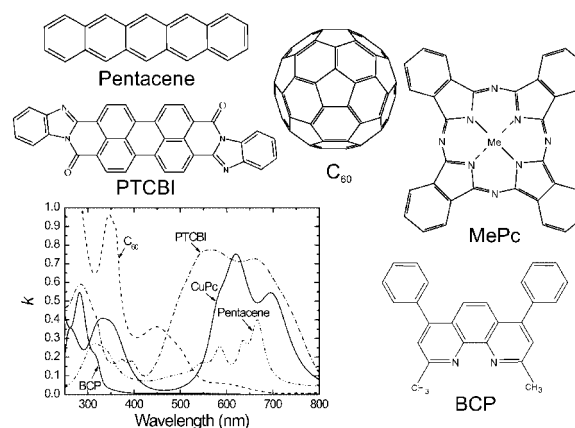


Figure 7. Typical small molecules used in the design of organic solar cells. Shown here are pentacene, metal phthalocyanine (MePc), 3,4,9,10-perylenetetracarboxylic bis-benzimidazole (PTCBI), bathocuproine (BCP), and fullerene C_{60} . The graph shows spectra of the imaginary part of the index of refraction, or extinction coefficient k , for a neat thin film of each material

Table I. Summary of optical and electrical properties of some small molecules used in organic solar cells, including ionization potential (IP), electron affinity (EA), optical energy gap (E_{opt}), mobility (μ), and exciton diffusion length (L_D).

References are given next to each value

Material ^a	IP (eV) ^b	EA (eV) ^c	E_{opt} (eV)	μ (cm ² /Vs)	L_D (nm)
C ₆₀	6.2 ^[77]	3.6 ^[77]	1.8	5.1×10^{-2} ^[78]	40 ± 5 ^[20]
CuPc	5.2 ^[79]	3.2 ^[79]	1.7	7.4×10^{-4} ^[78]	10 ± 3 ^[20]
NPD	5.5 ^[79]	1.7 ^[79]	3.1	3.0×10^{-4} ^[80]	12 ± 2 ^[81]
Pentacene	5.1 ^[79]	3.0 ^[79]	1.9	1.5×10^{-1} ^[82]	65 ± 16 ^[83]
PTCBI	6.2 ^[79]	3.6 ^[79]	1.7	2.4×10^{-6} ^[78]	3 ± 0.3 ^[20]

^a CuPc = copper phthalocyanine, NPD = *N,N'*-di-1-naphthyl-*N,N'*-diphenyl-1,1'-biphenyl-4,4'-diamine, and PTCBI = 3,4,9,10-perylenetetracarboxylic bisbenzimidazole.

^b Measured with ultraviolet photoemission spectroscopy with an error of ± 0.1 eV.

^c Measured with inverse photoemission spectroscopy with an error of ± 0.5 eV.

polyacenes,^{83–85} such as pentacene and tetracene, as well as the metal phthalocyanines (MePc), such as CuPc or ZnPc, are among the most studied donor materials. For acceptors, perylene compounds like 3,4,9,10-perylenetetracarboxylic bis-benzimidazole (PTCBI), as well as C₆₀, are commonly used. The electrical and optical properties of some common D and A materials are summarized in Table I. The L_D of the polyacenes and MePcs appear to be approximately 50 and 10 nm, respectively,^{20,83} whereas PTCBI and C₆₀ are 3 and 40 nm, respectively.²⁰ One reason for the large L_D of C₆₀ is due to the nearly unity intersystem crossing yield from singlet to triplet excitons⁸⁶ as well as its triplet lifetime of 10–100 μ s.⁸⁷ Bathocuproine (BCP) is also shown in Figure 7, and is used as an exciton blocking layer (EBL) in the double heterostructure device architecture, as described in Subsection “Double heterostructure.” It should be noted that material purity plays a crucial role in determining the efficiency of organic PV cells,^{88,89} and therefore materials should be purified via the vacuum thermal gradient sublimation technique prior to device fabrication.⁹⁰

Figure 7 plots the extinction coefficient, k , for neat thin films of these common materials, and each material absorbs at $\lambda \leq 800$ nm. To convert k to α , one can make use of the relation $\alpha = 4\pi k/\lambda$. From Equation (6) and Figure 5, it is seen that harvesting as large a portion of the solar spectrum is important to increase J_{SC} , particularly for the red and near-infrared spectral regions. For example absorbing light at $\lambda \leq 1 \mu\text{m}$ collects up to $\sim 70\%$ of the incident

power. Subsection “Other architectures” discusses methods for using organic materials to absorb and generate photocurrent in the infrared part of the solar spectrum.

Growth techniques

To produce thin films of small molecular weight materials for organic PV cells, there are a number of options available: organic molecular beam deposition (OMBD),⁹⁰ vacuum thermal evaporation (VTE),⁹⁰ and organic vapor phase deposition (OVPD).⁹¹ In the OMBD technique, material is deposited from a Knudsen cell or crucible in a chamber with a background pressure of $10^{-10} - 10^{-8}$ Torr (1 Torr = 133 Pa = 1.33 mbar). The VTE procedure involves placing purified organic material in a baffled Ta or W boat which is located between electrodes in a vacuum chamber with a base pressure of $10^{-7} - 10^{-6}$ Torr. When current is passed through the boat or crucible, the temperature is increased beyond the sublimation point of the material, and the material is evaporated, depositing everywhere on the chamber walls, as well as on the target substrate. A quartz crystal microbalance is used to monitor the growth rate (typically 0.5–3 $\text{\AA}/\text{s}$) and thickness of the film. The process of OVPD is fundamentally different from the other two growth techniques, in that an inert carrier gas, usually N₂, carries organic molecules through a furnace to deposit on a cooled substrate.⁹¹ In this respect, OVPD allows one to adjust multiple parameters such as carrier gas flow rate, substrate temperature, chamber temperature, and chamber pressure. Also, the heated chamber walls prevent material deposition, allowing for a more efficient use of source materials compared with VTE. It should be noted that these processes are solvent-free, and thus provide flexibility in device layer structure and material choice.

DEVICE ARCHITECTURES

The design of organic PV cells is driven by the unique properties of organic molecular solids. Specifically, for the majority of organic semiconducting materials, $L_D \ll 1/\alpha$. This implies that without paying particularly close attention to the architecture of the DA interface (see Subsection “Donor/acceptor interface”), it is difficult to achieve both a high η_A and η_{ED} . To further complicate the issue, charge carrier mobilities in organic materials are characteristically low, therefore maintaining minimal layer thickness is critical for

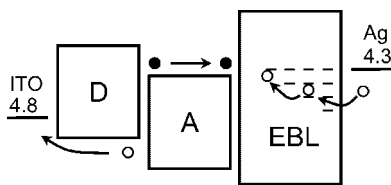


Figure 8. Schematic energy level diagram and proposed photovoltaic process for double heterostructure devices using an indium-tin-oxide (ITO) anode/donor (D)/acceptor (A)/exciton blocking layer (EBL)/Ag cathode structure. The D and A thicknesses are typically 20–50 nm, and the EBL approximately 10 nm

devices yielding low R_s . This section will highlight the roles that these parameters play in device design, and resulting architectures to optimize device performance will be presented.

Double heterostructure

To circumvent some issues pertaining to exciton confinement and absorption efficiency in organic solar cells, the double heterostructure architecture was introduced.⁹² This device is shown schematically in Figure 8, and consists of an EBL inserted between the acceptor-type molecular layer and the cathode. This layer serves a number of functions, the most important of which is to prevent damage to the photoactive layer during cathode deposition, thus eliminating exciton quenching at the acceptor/cathode interface. This damage can result in the formation of defect states within the organic layers which quench excitons as well as trap charge carriers, and can lead to a high contact resistance between the metal and organic layers, further degrading device performance. Therefore, materials such as C_{60} require EBLs to function⁹³ due to a large L_D which benefits from exciton confinement, whereas the original Tang structure with PTCBI as an acceptor did not have the same requirement.³⁷

Furthermore, at the metal surface and therefore at the metal/organic interface, the incident field intensity goes to zero. Therefore, the EBL should position the region of highest incident optical light intensity at the DA HJ, or at a distance of approximately $\lambda/4n$, where n is the index of refraction of the organic material, from the metal cathode. This will result in a higher exciton density at the photocurrent generating DA interface.

Some important criteria for potential EBL materials are: the material should be transparent across the solar

spectrum to act as a non-absorbing spacer between the photoactive region and the metal interface (see, for example, BCP absorption in Figure 7), and it must transport charge to ensure a low cell series resistance and high responsivity. Also, the ability to make relatively thick EBLs are practically important for fabricating large-area devices free of electrical shorts.

The most common EBL material used to date is that of BCP, but its large energy gap and high resistance make it unsuitable for use as a thick layer. Doping, or using low resistance compounds, has proven to be a route to using thicker EBL layers.^{93–95} Also, recently other materials have been proposed as EBL materials which are both organic and inorganic.^{96–98}

The multiple functions of the EBL layer are still a matter of continuing research.^{99,100} Recently, by comparing the device performance and interface energy levels of two different EBL materials,⁹³ it was confirmed that charge transport in BCP is due to damage induced during deposition of the cathode (shown in the EBL layer of Figure 8), while using an EBL with a low IP allows for hole transport to the C_{60} /EBL HJ and to direct recombination with electrons photogenerated in the acceptor layer, and this recombination mechanism was also determined for that of the BCP EBL. It is likely, however, that EBLs composed of electron conductive materials (see, for example, Reference [94]) are able to extract electrons from the acceptor layer. Further research has shown that $CuPc/C_{60}$ devices with planar DA HJs need an EBL, whereas mixed HJs (see Subsection “Donor/acceptor interface”) do not require one.¹⁰⁰ This in fact confirms the exciton blocking function, because the EBL does not need to confine excitons to the acceptor phase of the bulk HJ, which intrinsically possesses a high η_{ED} owing to the large DA interfacial area.

Donor/acceptor interface

In order to increase the efficiency of organic solar cells, the DA interface where photocurrent is generated is the focal point. Specifically, to increase J_{SC} , one method is to increase η_{ED} by reducing the average distance between donor and acceptor molecules. To accomplish this goal without reducing the overall thickness of the device active layers, blends of donor and acceptor molecules have been used to form an interpenetrating DA network, or the so-called mixed, or bulk HJ,^{101,102} illustrated in Figure 9(b). Compared with the planar HJ introduced by Tang, formed between homogeneous donor and acceptor layers and shown in Figure 9(a),

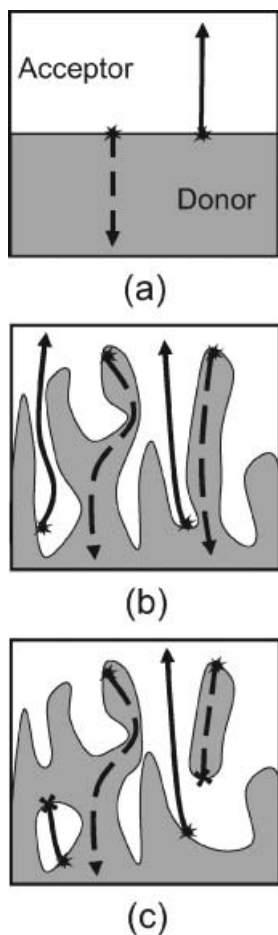


Figure 9. Representation of donor/acceptor interface architecture possibilities: (a) a planar heterojunction, formed between thin films of donor and acceptor materials; (b) an optimal bulk heterojunction, where there is complete phase separation of donor to one side and acceptor to the other side of the device structure; and (c) a non-ideal bulk heterojunction, where isolated regions of donor and/or acceptor phases prevent the collection of photogenerated charges. Dashed (solid) lines correspond to hole (electron) transport, and the arrow ("x") represents continuing (terminated) charge carrier flow

a bulk HJ expands the photocurrent generation region of the device, allowing excitons a higher probability to reach a nearby DA interface where they can dissociate. In an optimal arrangement,¹⁰³ the width of the phases in the interdigitated structure should be on the order of $2L_D$, ensuring that excitons generated in the center of the material have a good chance of dissociating while at the same time providing low resistance pathways for charge transport.

In practice, however, achieving such a structure is difficult. Co-deposited mixtures of donor and acceptor small molecules have been used to achieve a bulk HJ structure^{78,104–109} reaching $\eta_p \approx 3.5\%$ under 1 sun (AM1.5G) illumination.¹⁰⁶ However, the performance of bulk HJ PV cells relies critically on the microstructure of the mixture. For example co-evaporation does not lead to an idealized structure,^{78,104,106–108} but one where isolated phases of material (as in Figure 9(c)) exist that prevent efficient charge collection. In the worst case scenario (not pictured), co-evaporation leads to uniform molecular scale mixing of the two molecules with minimal evidence of phase separation.⁷⁸

When trying to understand the performance of solar cells based upon mixed DA films, it is therefore important to know their optical, morphological, and electrical properties.^{78,107} Through space charge limited current mobility measurements, it was found that mixed layers were characterized by lower charge carrier mobilities than neat films. This is shown in Figure 10, where we see that the hole mobility in a 1:1 CuPc:C₆₀ film is decreased by approximately a factor of 100 compared with the neat CuPc value, and much lower when compared with the electron mobility. This, along with the fact that

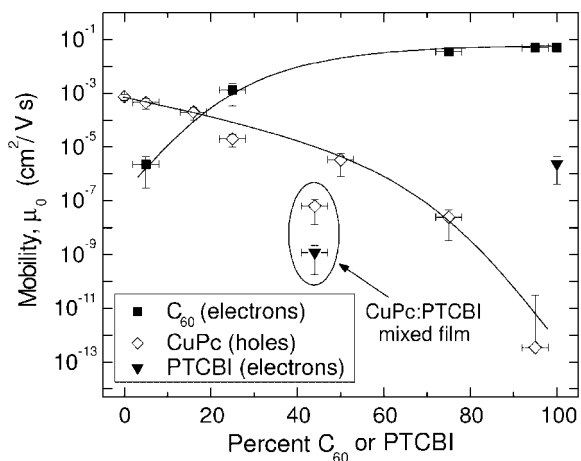


Figure 10. The zero field mobility, μ_0 , for electrons (filled symbols) and holes (open symbols) in various pure and mixed films containing CuPc (diamonds), C₆₀ (squares), and PTCBI (triangles), versus percent of C₆₀ or PTCBI in the mixture. The mixed films are all CuPc:C₆₀, except for the two circled symbols, which correspond to 5:4 CuPc:PTCBI. The lines serve as guides to the eye. Reprinted with permission from Reference [78]. Copyright 2005, American Institute of Physics

device performance is optimized for a 1:1 CuPc:C₆₀ mixture suggests that the cells are ultimately limited by hole transport through the mixture. Furthermore, the drop in hole mobility is at least 10 times larger when mixing CuPc and PTCBI as compared with the CuPc:C₆₀ mixture (see Figure 10). This is in agreement with previous device results, where homogeneously mixed CuPc:PTCBI devices show poor transport of photogenerated carriers,^{105,110} as indicated by the low cell power conversion efficiencies. Annealing mixed films was found to induce phase separation of the constituents, thus improving charge transport¹⁰⁵ and device performance. This mobility decrease in mixed DA thin films is consistent with the fact that the mean distance between neighboring molecules of the same species is larger than in a homogeneous layer, and thus hopping mobility decreases. Also, these space charge limited mobility trends were recently confirmed with field effect transistor mobility measurements,¹¹¹ which gives further evidence that these mixtures are homogeneous and transport is isotropic.

The challenge in applying these mixed molecular heterojunctions is therefore in balancing the absorption needed for photocurrent generation with the reduced charge transport properties of the mixed layer. This is because maintaining good charge transport and a low R_s is an important factor in creating efficient organic PV cells³⁵ with high FF, and reducing the chance of recombination of the photogenerated charges within the mixture. This can be accomplished by using a hybrid planar-mixed-molecular heterojunction (PM-HJ), consisting of a mixed DA layer sandwiched between homogeneous donor and acceptor layers.^{23,110} An optimized hybrid PM-HJ structure has a thinner mixed layer than a bulk HJ cell, and the thicknesses of the homogeneous layers are approximately equal to L_D in each respective layer. In this way, the device has the high η_{ED} of a mixed HJ, and the low resistance to charge transport of a planar HJ. Under 1–4 suns simulated AM1.5G solar illumination, such structures comprising CuPc and C₆₀ achieved a power conversion efficiency of $\eta_P = 5.0\%$.²³

In an effort to recover a more nearly ideal structure in the thermally co-evaporated thin film, annealing a CuPc:PTCBI blend to temperatures of ~ 500 K was shown to induce phase separation of the two materials and increase η_{CC} .¹⁰⁵ Similarly, it has also been shown that annealing a pentacene/C₆₀⁸⁴ or tetracene/C₆₀¹¹³ planar HJ resulted in better performing devices. While the mechanism for this enhancement is not fully

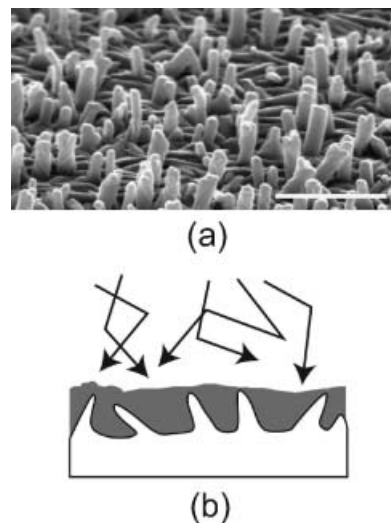


Figure 11. (a) Scanning electron microscope image of a CuPc film grown using OVPD, showing short, needle-like crystals of CuPc extending out of the CuPc film. Scale bar = 500 nm. (b) Representation of the gap-filling capability of the OVPD process to assemble a bulk heterojunction, due to a short mean-free path and increased surface diffusion. Reprinted with permission from Macmillan Publishers, Ltd. Reference [112], Copyright 2005

understood, it could be a result of increased order within the active layers. Alternatively, it is also possible to grow the D and A layers via the OVPD growth technique, to directly form a bulk HJ structure where D and A layers are phase separated.¹¹² This is shown in Figure 11, where it is possible to control the growth mode of a CuPc film on ITO such that crystalline needles of CuPc extend out of the CuPc film. Following the growth of CuPc, it was shown that the OVPD process was also successful in filling the spaces within this rough CuPc film owing to the short mean free path length inherent to the OVPD process (see Subsection “Growth techniques”), whereas growth via a UHV process would result in voids in the film.¹¹² Constructing such a structure resulted in an increase in device efficiency of a CuPc/PTCBI solar cell from 1.1% to 2.7%.

Tandem cell

Another way to ensure a high η_A while keeping the thickness of the D and A layers to approximately L_D is by using a tandem cell architecture, originally developed by Hiramoto *et al.*¹¹⁴ for organic PV cells, and consisting of a series connection of a number of

individual DA junctions with a charge recombination zone (CRZ) separating each subcell in the stack. By maintaining a similar total device thickness, a stacked cell compensates for the reduction in η_A per device. The stacked cell also results in an increase in V_{OC} due to the addition of the photovoltage of each individual subcell. Because of these potential benefits, there has been intensive work into trying to optimize the architecture of such a structure applied to cells with small molecules,^{94,115–120} polymers,^{121–125} combinations of both,^{126,127} as well as to DSSCs.¹²⁸

Figure 12(a) shows a schematic diagram of a tandem organic PV cell. The front (PV1) and back cell (PV2) are separated by the CRZ. The operation proceeds as follows: light absorption generates excitons in PV1 and PV2. After exciton dissociation in the subcells, the hole in PV1 and electron in PV2 are collected at the adjacent electrodes. To prevent build-up of charge within the cells, the electron in PV1 and hole in PV2 diffuse to the CRZ where they recombine. The main challenge to realizing tandem cells is in balancing the photocurrent from each cell as the current in the series-connected device is limited by the smallest subcell current. This can be accomplished by varying the thicknesses or the material selection of the various device layers, but becomes complicated due to optical interference effects. This is demonstrated in Figure 12(b), where incident light with $\lambda = 450$ nm (solid line) and $\lambda = 650$ nm (dashed line) have intensity maxima at different positions within the organic layer structure. Therefore, to optimize device performance, one needs to place materials with absorption in different regions of the solar spectrum at different points within the tandem structure.

Yakimov and Forrest¹¹⁵ reported a tandem PV cell consisting of multiple CuPc/PTCBI DA HJs, with each DA pair separated by a thin Ag cluster CRZ. This, along with Au clusters, are amongst the most commonly used CRZ materials. The observed power efficiency of their tandem cell device was 2.5% whereas for a single CuPc/PTCBI cell, $\eta_P = 1.1\%$. It was found that the optical field enhancement due to surface plasmon generation on the metal clusters in the CRZ is responsible for the higher-than-expected efficiencies observed in their tandem organic PV cells.¹¹⁶ Alternatively, an effective means to space the subcells apart is by employing the *p-i-n* device architecture,⁹⁴ shown schematically in Figure 13(a). Here, *p*- and *n*-type wide-gap transport layers which optimally do not absorb the incident light are used to

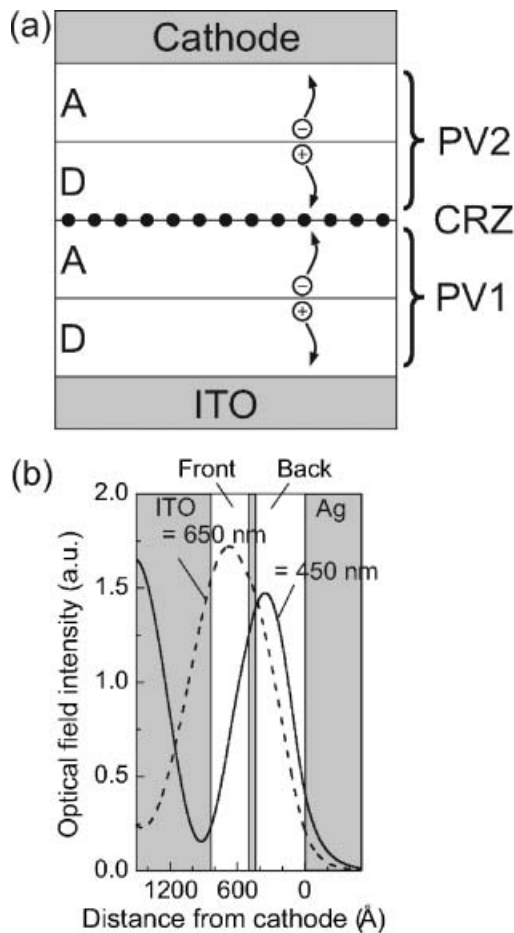


Figure 12. (a) Schematic of a tandem organic photovoltaic cell. The donor (D) layer and acceptor (A) layer of each device (PV1 and PV2) are labeled, as is the charge recombination zone (CRZ) between PV1 and PV2. The schematic shows a representation of current generation, where dissociation of excitons at the DA interfaces leads to a hole in PV1 and electron in PV2 which contribute to photocurrent. The excess electron in PV1 and hole in PV2 recombine at the CRZ to prevent cell charging. (b) Optical field intensities at $\lambda = 450$ nm (solid line) and $\lambda = 650$ nm (dashed line) calculated as functions of the distance from the Ag cathode. Reprinted with permission from Reference [117]. Copyright 2004, American Institute of Physics

spatially separate the mixed, or *i*, layers that generate photocurrent. The resulting *J-V* characteristics for the single and tandem *p-i-n* device are shown in Figure 13(b),¹¹⁹ with $\eta_P = 2.1\%$ for the single cell and 3.8% for the tandem device. Here, the current for the tandem cell is lower than that of the single cell, likely due to a combination of a current mismatch

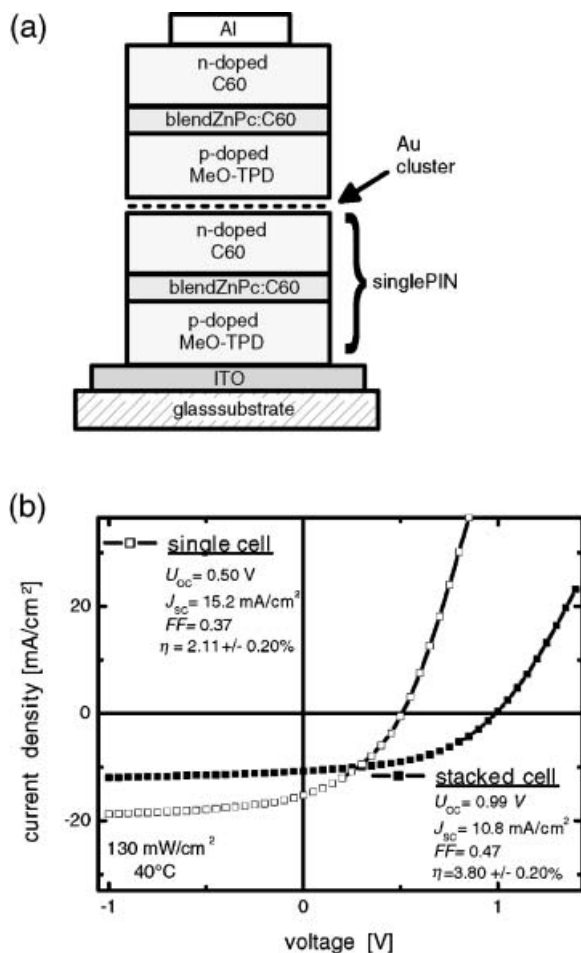


Figure 13. (a) Concept of a stacked *p-i-n* organic solar cell with active layers sandwiched between *p*- and *n*-type wide-gap transport layers. (b) *J*-*V* characteristics of single and tandem *p-i-n* solar cells under 130 mW/cm² simulated AM1.5 solar illumination. The single cell is identical to the bottom cell in the tandem configuration and prepared simultaneously. The performance parameters are given. Reprinted with permission from Reference [119] Copyright 2005, American Institute of Physics

as well as the fact that both *i* layers are composed of the same DA combination. However, the observed doubling in V_{OC} meant an overall increase in η_P . A tandem cell composed of two hybrid PM-HJ cells was also demonstrated, where $\eta_P = 5.7\%$ ¹¹⁷ was achieved, approximately 10% higher than that of a single cell.²³ Again, the reason for a less-than-doubling in η_P is similar to that of the *p-i-n* device just discussed. In fact, it is an almost universal observation that optimized organic tandem cells have lower J_{SC} values than optimized single cells. If the efficiency

is improved, which is difficult to achieve for the reasons discussed above, it is due to the increased V_{OC} . Improved performance is therefore expected from a fully “asymmetric” tandem device, with subcells operating in different regions of the solar spectrum.

Other architectures

We also consider the use of other, novel architectures employed in small-molecular weight based solar cells developed in an effort to try to increase device efficiency. For example, in order to incorporate low mobility materials into an efficient device structure, an architecture analogous to that used for quantum dot light-emitting devices¹²⁹ was developed. In this architecture,¹³⁰ an ultrathin SnPc molecular layer was deposited in between CuPc and C₆₀ films. The SnPc layer has a very high absorption coefficient which extends to $\lambda \approx 1000$ nm. Therefore, this represents an important step toward achieving organic solar cells which absorb in the near infrared portion of the solar spectrum. The optimized device with a 5 nm thick SnPc layer had a power conversion efficiency of 1.0% and a FF = 0.5. Therefore, it was important to control the SnPc layer thickness such that its low hole mobility did not negatively impact device performance. Another method for extending the absorption range of organic solar cells is through the use of a luminescent collector.¹³¹ This collector does not directly generate charge, but rather absorbs light which would otherwise not be absorbed in the cell, and emits light within the absorption spectrum of the solar cell active layers. By implementing such a collector, a 15% increase in J_{SC} was achieved.¹³¹

A couple of new architectures centered around influencing the optical intensity at the DA interface have also been demonstrated. The semitransparent organic PV cell^{124,132} is one of these, and shows promise for use as a power-generating device on transparent substrates for architectural or portable applications. In this device structure, transparent contacts are used as both the anode and cathode. This has important consequences for the optical design of such cells, as the optical interference effects are drastically different. The weak cavity implies that multiple devices operating in different wavelength regions can be stacked without the strict requirements of optical design that are unavoidable in the design of opaque tandem cells with a reflecting cathode (see Subsection “Tandem cell”). However, it remains an open question whether the semitransparent structure can realize this potential

benefit and operate as efficiently as cells with metal cathodes. In another approach, an external dielectric coating¹³³ applied to a semitransparent, top-light harvesting cathode¹³⁴ was shown to increase the light intensity at the DA interface as well as remove the need for an ITO anode.

DEVICE STABILITY

Device stability remains a very important issue concerning the commercialization of organic solar cells, and it is estimated that lifetimes of at least 5 years are necessary for practical devices.¹³⁵ Despite this fact, to date there have been relatively few studies of the lifetime of organic solar cells based upon small molecular weight materials,^{98,136,137} where lifetimes of greater than 1500 h ($\eta_p = 50\%$ of original value) have been demonstrated for unencapsulated devices. More recently, the shelf lifetime of a pentacene/ C_{60} cell encapsulated with an Al_2O_3 film deposited by atomic layer deposition was shown to degrade by 6% over a period of 6100 h (≈ 8.5 months), compared to a lifetime of < 10 h for an unencapsulated cell.¹³⁸ Therefore, to increase the stability of such devices requires careful selection of D, A, EBL, electrode, and encapsulation materials.

Nevertheless, the lifetime of large-area polymer-based bulk HJ devices has recently been projected to be $> 10\,000$ h, albeit for a rather low-performance device.¹³⁹ Dye-sensitized solar cells have also shown to be very stable during operation, with lifetimes in the 5–10 year range.^{140–142} Furthermore, organic light emitting diodes made with small molecular weight semiconductors have demonstrated lifetimes of $> 10\,000$ h.¹⁴³ These results are therefore promising for small molecule-based PV cells to exhibit similar and ultimately sufficient lifetimes as well.

CONCLUSIONS

This review has sought to introduce the device physics underlying organic solar cells based upon donor/acceptor interfaces. Following this introduction, we leveraged that understanding toward the various device architectures, materials, and growth techniques that are employed to exploit the unique material characteristics of small molecular weight organic semiconductors, in particular strong absorption and low charge carrier mobilities. To improve device

performance, the identification of high performance donor/acceptor pairs is important to simultaneously optimize open-circuit voltage and short-circuit current. Furthermore, the development of high-efficiency tandem solar cells was discussed, and the continued improvement of this device structure will rely upon finding new and improved materials along with careful optical design to ensure that the active layers are placed at the point of maximum incident light intensity.

Ultimately, to realize the commercial application of organic solar cells, the challenge is in developing large-area modules with long operational lifetimes, high production yields, low production costs, and high efficiency. Once these parameters are known, possible applications, whether it be for stationary, building-integrated projects, or for portable power generation on lightweight plastic substrates, can be targeted. The recent increases in efficiency along with the growing research community in organic solar cells indicate that commercially viable efficiencies of greater than 10% seem within reach. Achieving these goals will undoubtedly require a multidisciplinary approach from chemistry, physics, materials science, and engineering communities.

Acknowledgments

The authors would like to thank D. Cheyns for providing some molecular structures and optical constants and R. J. Holmes for some molecular structures and helpful discussions. Also thanks to F. Yang, S. R. Forrest, and J. Drechsel for kindly providing figures.

REFERENCES

1. Forrest SR. The path to ubiquitous and low-cost organic electronic appliances on plastic. *Nature* 2004; **428**(6986): 911–918.
2. Singh TB, Sariciftci NS. Progress in plastic electronics devices. *Annual Reviews of Materials Research* 2006; **36**: 199–230.
3. Malliaras G, Friend R. An organic electronics primer. *Physics Today* 2005; **58**(5): 53–58.
4. Forrest SR. The road to high efficiency organic light emitting devices. *Organic Electronics* 2003; **4**(2–3): 45–48.
5. Khan RUA, Hunziker C, Gunter P. Perspectives on organic light-emitting diodes for display applications. *Journal of Materials Science: Materials in Electronics* 2006; **17**(6): 467–474.

6. D'Andrade BW, Forrest SR. White organic light-emitting devices for solid-state lighting. *Advanced Materials* 2004; **16**(18): 1585–1595.
7. Dimitrakopoulos CD, Malenfant PRL. Organic thin film transistors for large area electronics. *Advanced Materials* 2002; **14**(2): 99–117.
8. Sirringhaus H. Device physics of solution-processed organic field-effect transistors. *Advanced Materials* 2005; **17**(20): 2411–2425.
9. Shaheen SE, Ginley DS, Jabbour GE. Organic-based photovoltaics. Toward low-cost power generation. *MRS Bulletin* 20.
10. Gledhill SE, Scott B, Gregg BA. Organic and nano-structured composite photovoltaics: an overview. *Journal of Materials Research* 2005; **20**(12): 3167–3179.
11. Hoppe H, Sariciftci NS. Organic solar cells: an overview. *Journal of Materials Research* 2004; **19**(7): 1924–1945.
12. Gratzel M. Perspectives for dye-sensitized nanocrystalline solar cells. *Progress in Photovoltaics: Research and Applications* 2000; **8**: 171–185.
13. Schmidt-Mende L, Bach U, Humphry-Baker R, Horiuchi T, Miura H, Ito S, Uchida S, Gratzel M. Organic dye for highly efficient solid-state dye-sensitized solar cells. *Advanced Materials* 2005; **17**: 813.
14. Coakley KM, Liu YX, Goh C, McGehee MD. Ordered organic-inorganic bulk heterojunction photovoltaic cells. *MRS Bulletin* 2005; **30**(1): 37–40.
15. Milliron DJ, Gur I, Alivisatos AP. Hybrid organic—nanocrystal solar cells. *MRS Bulletin* 2005; **30**(1): 41–44.
16. Dennler G, Sariciftci NS. Flexible conjugated polymer-based plastic solar cells: from basics to applications. *Proceedings of the IEEE* 2005; **93**(8): 1429–1439.
17. Coakley KM, McGehee MD. Conjugated polymer photovoltaic cells. *Chemistry of Materials* 2004; **16**(23): 4533–4542.
18. Janssen RAJ, Hummelen JC, Saricifti NS. Polymer-fullerene bulk heterojunction solar cells. *MRS Bulletin* 2005; **30**(1): 33–36.
19. Forrest SR. The limits to organic photovoltaic cell efficiency. *MRS Bulletin* 2005; **30**(1): 28–32.
20. Peumans P, Yakimov A, Forrest SR. Small molecular weight organic thin-film photodetectors and solar cells. *Journal of Applied Physics* 2003; **93**(7): 3693–3723.
21. Li G, Shrotriya V, Huang JS, Yao Y, Moriarty T, Emery K, Yang Y. High-efficiency solution processable polymer photovoltaic cells by self-organization of polymer blends. *Nature Materials* 2005; **4**(11): 864–868.
22. Ma WL, Yang CY, Gong X, Lee K, Heeger AJ. Thermally stable, efficient polymer solar cells with nanoscale control of the interpenetrating network morphology. *Advanced Functional Materials* 2005; **15**(10): 1617–1622.
23. Xue J, Rand BP, Uchida S, Forrest SR. A hybrid planar-mixed molecular heterojunction photovoltaic cell. *Advanced Materials* 2005; **17**(1): 66–70.
24. ISI Web of Science search on March 6, 2007 for: (organic OR plastic OR polymer OR dye OR molecular) AND (solar OR photovoltaic) AND cell NOT “beam epitaxy” NOT “chemical vapor deposition” NOT GaAs NOT MOCVD NOT CVD.
25. Gregg BA, Hanna MC. Comparing organic to inorganic photovoltaic cells: theory, experiment, and simulation. *Journal of Applied Physics* 2003; **93**(6): 3605–3614.
26. Nelson J. *The Physics of Solar Cells*. Imperial College Press: London, 2003.
27. Bube R, Fahrenbruch A. *Advances in Electronics and Electron Physics*, Vol. 56. Academic Press: New York, 1981.
28. Rand BP, Burk DP, Forrest SR. Offset energies at organic semiconductor heterojunctions and their influence on the open-circuit voltage of thin-film solar cells. *Physical Review B* 2007; **75**: 115327.
29. Yoo S, Domercq B, Kippelen B. Intensity-dependent equivalent circuit parameters of organic solar cells based on pentacene and C-60. *Journal of Applied Physics* 2005; **97**(10): 103706.
30. Moliton A, Nunzi JM. How to model the behaviour of organic photovoltaic cells. *Polymer International* 2006; **55**(6): 583–600.
31. Nelson J, Kirkpatrick J, Ravirajan P. Factors limiting the efficiency of molecular photovoltaic devices. *Physical Review B* 2004; **69**(3): 035337.
32. Peumans P, Forrest SR. Separation of geminate charge-pairs at donor-acceptor interfaces in disordered solids. *Chemical Physics Letters* 2004; **398**(1–3): 27–31.
33. Glatthaar M, Riede M, Keegan N, Sylvester-Hvid K, Zimmermann B, Niggemann M, Hinsch A, Gombert A. Efficiency limiting factors of organic bulk heterojunction solar cells identified by electrical impedance spectroscopy. *Solar Energy Materials and Solar Cells* 2007; **91**(5): 390–393.
34. Reynaert J, Arkhipov VI, Heremans P, Poortmans J. Photomultiplication in disordered unipolar organic materials. *Advanced Functional Materials* 2006; **16**(6): 784–790.
35. Xue J, Uchida S, Rand BP, Forrest SR. 4.2% efficient organic photovoltaic cells with low series resistances. *Applied Physics Letters* 2004; **84**(16): 3013–3015.
36. Chamberlain GA. Organic solar-cells—a review. *Solar Cells* 1983; **8**(1): 47–83.
37. Tang CW. 2-layer organic photovoltaic cell. *Applied Physics Letters* 1986; **48**(2): 183–185.
38. Knupfer M. Exciton binding energies in organic semiconductors. *Applied Physics A* 2003; **77**(5): 623–626.

39. Hill IG, Kahn A, Soos ZG, Pascal RA. Charge-separation energy in films of pi-conjugated organic molecules. *Chemical Physics Letters* 2000; **327**(3–4): 181–188.
40. Arkhipov VI, Heremans P, Bassler H. Why is exciton dissociation so efficient at the interface between a conjugated polymer and an electron acceptor? *Applied Physics Letters* 2003; **82**(25): 4605–4607.
41. Silinsh EA, Capek V. *Organic Molecular Crystals*. AIP Press: Woodbury, NY, 1994.
42. Onsager L. Initial recombination of ions. *Physical Review* 1938; **54**: 554–557.
43. ASTM Standards E1021, E948, and E973 (American Society for Testing and Materials, W. Conshohocken, PA).
44. Shrotriya V, Li G, Yao Y, Moriarty T, Emery K, Yang Y. Accurate measurement and characterization of organic solar cells. *Advanced Functional Materials* 2006; **16**(15): 2016–2023.
45. Pettersson LAA, Roman LS, Inganäs O. Modeling photocurrent action spectra of photovoltaic devices based on organic thin films. *Journal of Applied Physics* 1999; **86**(1): 487–496.
46. Terao Y, Sasabe H, Adachi C. Correlation of hole mobility, exciton diffusion length, and solar cell characteristics in phthalocyanine/fullerene organic solar cells. *Applied Physics Letters* 2007; **90**(10): 103515.
47. Scully S, McGehee M. Effects of optical interference and energy transfer on exciton diffusion length measurements in organic semiconductors. *Journal of Applied Physics* 2006; **100**: 034907.
48. Lemaire V, Steel M, Beljonne D, Bredas JL, Cornil J. Photoinduced charge generation and recombination dynamics in model donor/acceptor pairs for organic solar cell applications: a full quantum-chemical treatment. *Journal of the American Chemical Society* 2005; **127**(16): 6077–6086.
49. Marcus RA, Sutin N. Electron transfers in chemistry and biology. *Biochimica et Biophysica Acta* 1985; **811**(3): 265–322.
50. Sun SS. Optimum energy levels and offsets for organic donor/acceptor binary photovoltaic materials and solar cells. *Materials Science and Engineering B* 2005; **116**(3): 251–256.
51. Bredas JL, Beljonne D, Coropceanu V, Cornil J. Charge-transfer and energy-transfer processes in pi-conjugated oligomers and polymers: a molecular picture. *Chemical Reviews* 2004; **104**(11): 4971–5003.
52. Mutolo KL, Mayo EI, Rand BP, Forrest SR, Thompson ME. Enhanced open-circuit voltage in subphthalocyanine/C-60 organic photovoltaic cells. *Journal of the American Chemical Society* 2006; **128**(25): 8108–8109.
53. Schulze K, Uhrich C, Schuppel R, Leo K, Pfeiffer M, Brier E, Reinold E, Bauerle P. Efficient vacuum-deposited organic solar cells based on a new low-bandgap oligothiophene and fullerene C-60. *Advanced Materials* 2006; **18**(21): 2872–2875.
54. Singh VP, Singh RS, Parthasarathy B, Aguilera A, Anthony J, Payne M. Copper-phthalocyanine-based organic solar cells with high open-circuit voltage. *Applied Physics Letters* 2005; **86**(8): 082106.
55. Liu P, Li Q, Huang MS, Pan WZ, Deng WJ. High open circuit voltage organic photovoltaic cells based on oligothiophene derivatives. *Applied Physics Letters* 2006; **89**(21): 213501.
56. Scharber MC, Wühlbacher D, Koppe M, Denk P, Waldauf C, Heeger AJ, Brabec CJ. Design rules for donors in bulk-heterojunction solar cells—towards 10% energy-conversion efficiency. *Advanced Materials* 2006; **18**(6): 789–794.
57. Brabec CJ, Cravino A, Meissner D, Sariciftci NS, Fromherz T, Rispeens MT, Sanchez L, Hummelen JC. Origin of the open circuit voltage of plastic solar cells. *Advanced Functional Materials* 2001; **11**(5): 374–380.
58. Brabec CJ, Cravino A, Meissner D, Sariciftci NS, Rispeens MT, Sanchez L, Hummelen JC, Fromherz T. The influence of materials work function on the open circuit voltage of plastic solar cells. *Thin Solid Films* 2002; **403**: 368–372.
59. Deng XY, Zheng LP, Yang CH, Li YF, Yu G, Cao Y. Polymer photovoltaic devices fabricated with blend MEHPPV and organic small molecules. *Journal of Physical Chemistry B* 2004; **108**(11): 3451–3456.
60. Gadisa A, Svensson M, Andersson MR, Inganäs O. Correlation between oxidation potential and open-circuit voltage of composite solar cells based on blends of polythiophenes/fullerene derivative. *Applied Physics Letters* 2004; **84**(9): 1609–1611.
61. Kietzke T, Egbe DAM, Horhold HH, Neher D. Comparative study of M3EH-PPV-based bilayer photovoltaic devices. *Macromolecules* 2006; **39**(12): 4018–4022.
62. Sylvester-Hvid KO. Two-dimensional simulations of CuPc-PTCDA solar cells: the importance of mobility and molecular pi stacking. *Journal of Physical Chemistry B* 2006; **110**(6): 2618–2627.
63. Aernouts T, Vanlaeke P, Geens W, Poortmans J, Heremans P, Borghs S, Mertens R, Andriessen R, Leenders L. Printable anodes for flexible organic solar cell modules. *Thin Solid Films* 2004; **451**: 22–25.
64. Huang J, Wang X, Kim Y, deMello AJ, Bradley DDC, Demello JC. High efficiency flexible ITO-free polymer/fullerene photodiodes. *Physical Chemistry Chemical Physics* 2006; **8**(33): 3904–3908.
65. Kushto GP, Kim WH, Kafafi ZH. Flexible organic photovoltaics using conducting polymer electrodes. *Applied Physics Letters* 2005; **86**(9): 093502.
66. Pandey AK, Nunzi JM. Efficient flexible and thermally stable pentacene/C-60 small molecule based organic

- solar cells. *Applied Physics Letters* 2006; **89**(21): 213506.
67. Yang F, Forrest SR. Organic solar cells using transparent SnO₂-F anodes. *Advanced Materials* 2006; **18**(15): 2018–2022.
 68. Owen J, Son MS, Yoo KH, Ahn BD, Lee SY. Organic photovoltaic devices with ga-doped zno electrode. *Applied Physics Letters* 2007; **90**(3): 033512.
 69. Admassie S, Zhang FL, Manoj AG, Svensson M, Andersson MR, Inganas O. A polymer photodiode using vapour-phase polymerized PEDOT as an anode. *Solar Energy Materials and Solar Cells* 2006; **90**(2): 133–141.
 70. Pasquier AD, Unalan HE, Kanwal A, Miller S, Chhowalla M. Conducting and transparent single-wall carbon nanotube electrodes for polymer-fullerene solar cells. *Applied Physics Letters* 2005; **87**(20): 203511.
 71. Rowell MW, Topinka MA, McGehee MD, Prall HJ, Dennler G, Sariciftci NS, Hu LB, Gruner G. Organic solar cells with carbon nanotube network electrodes. *Applied Physics Letters* 2006; **88**(23): 233506.
 72. van de Lagemaat J, Barnes TM, Rumbles G, Shaheen SE, Coutts TJ, Weeks C, Levitsky I, Peltola J, Glatkowski P. Organic solar cells with carbon nanotubes replacing In₂O₃:Sn as the transparent electrode. *Applied Physics Letters* 2006; **88**(23): 233503.
 73. Gruner G. Carbon nanotube films for transparent and plastic electronics. *Journal of Materials Chemistry* 2006; **16**(35): 3533–3539.
 74. Ulbricht R, Jiang X, Lee S, Inoue K, Zhang M, Fang S, Baughman R, Zakhidov A. Polymeric solar cells with oriented and strong transparent carbon nanotube anode. *Physica Status Solidi B* 2006; **243**(13): 3528–3532.
 75. Armstrong NR, Carter C, Donley C, Simmonds A, Lee P, Brumbach M, Kippelen B, Domercq B, Yoo SY. Interface modification of ITO thin films: organic photovoltaic cells. *Thin Solid Films* 2003; **445**(2): 342–352.
 76. Khodabakhsh S, Sanderson BM, Nelson J, Jones TS. Using self-assembling dipole molecules to improve charge collection in molecular solar cells. *Advanced Functional Materials* 2006; **16**(1): 95–100.
 77. Benning PJ, Poirier DM, Ohno TR, Chen Y, Jost MB, Stepniak F, Kroll GH, Weaver JH, Fure J, Smalley RE. C-60 and C-70 fullerenes and potassium fullerides. *Physical Review B* 1992; **45**(12): 6899–6913.
 78. Rand BP, Xue J, Uchida S, Forrest SR. Mixed donor-acceptor molecular heterojunctions for photovoltaic applications. I. Material properties. *Journal of Applied Physics* 2005; **98**(12): 124902.
 79. Kahn A, Koch N, Gao WY. Electronic structure and electrical properties of interfaces between metals and pi-conjugated molecular films. *Journal of Polymer Science Part A* 2003; **41**(21): 2529–2548.
 80. Nguyen ND, Schmeits M, Loebel HP. Determination of charge-carrier transport in organic devices by admittance spectroscopy: application to hole mobility in alpha-NPD. *Physical Review B* 2007; **75**(7): 075307.
 81. Rand BP. Unpublished results.
 82. Steudel S, Myny K, Arkhipov V, Deibel C, De Vusser S, Genoe J, Heremans P. 50 MHz rectifier based on an organic diode. *Nature Materials* 2005; **4**(8): 597–600.
 83. Yoo S, Domercq B, Kippelen B. Efficient thin-film organic solar cells based on pentacene/C-60 heterojunctions. *Applied Physics Letters* 2004; **85**(22): 5427–5429.
 84. Mayer AC, Lloyd MT, Herman DJ, Kasen TG, Malliaras GG. Postfabrication annealing of pentacene-based photovoltaic cells. *Applied Physics Letters* 2004; **85**(25): 6272–6274.
 85. Chu CW, Shao Y, Shrotriya V, Yang Y. Efficient photovoltaic energy conversion in tetracene-C-60 based heterojunctions. *Applied Physics Letters* 2005; **86**(24): 243506.
 86. Terazima M, Hirota N, Shinohara H, Saito Y. Photothermal investigation of the triplet-state of C60. *Journal of Physical Chemistry* 1991; **95**(23): 9080–9085.
 87. Sassara A, Zerza G, Chergui M. Phosphorescence of C-60 in rare gas matrices. *Chemical Physics Letters* 1996; **261**(3): 213–220.
 88. Drechsel J, Petrich A, Koch M, Pfuetzner S, Meerheim R, Scholz S, Walzer K, Pfeiffer M, Leo K. Influence of material purification by vacuum sublimation on organic optoelectronic device performance. *SID Symposium Digest of Technical Papers* 2006; **37**(1): 1692–1695.
 89. Salzman RF, Xue J, Rand BP, Alexander A, Thompson ME, Forrest SR. The effects of copper phthalocyanine purity on organic solar cell performance. *Organic Electronics* 2005; **6**(5–6): 242–246.
 90. Forrest SR. Ultrathin organic films grown by organic molecular beam deposition and related techniques. *Chemical Reviews* 1997; **97**(6): 1793–1896.
 91. Shtein M, Gossenberger HF, Benziger JB, Forrest SR. Material transport regimes and mechanisms for growth of molecular organic thin films using low-pressure organic vapor phase deposition. *Journal of Applied Physics* 2001; **89**(2): 1470–1476.
 92. Peumans P, Bulovic V, Forrest SR. Efficient photon harvesting at high optical intensities in ultrathin organic double-heterostructure photovoltaic diodes. *Applied Physics Letters* 2000; **76**(19): 2650–2652.
 93. Rand BP, Li J, Xue J, Holmes RJ, Thompson ME, Forrest SR. Organic double-heterostructure photovoltaic cells employing thick tris(acetylacetonato)ruthenium(III) exciton-blocking layers. *Advanced Materials* 2005; **17**(22): 2714–2718.
 94. Maennig B, Drechsel J, Gebeyehu D, Simon P, Kozlowski F, Werner A, Li F, Grundmann S, Sonntag S, Koch M, Leo K, Pfeiffer M, Hoppe H, Meissner D,

- Sariciftci NS, Riedel I, Dyakonov V, Parisi J. Organic p-i-n solar cells. *Applied Physics A* 2004; **79**(1): 1–14.
95. Suemori K, Miyata T, Yokoyama M, Hiramoto M. Organic solar cells protected by very thick naphthalene tetracarboxylic anhydride films. *Applied Physics Letters* 2004; **85**(25): 6269–6271.
96. Hansel H, Zettl H, Krausch G, Kisselev R, Thelakkat M, Schmidt HW. Optical and electronic contributions in double-heterojunction organic thin-film solar cells. *Advanced Materials* 2003; **15**(24): 2056–2060.
97. Chan MY, Lee CS, Lai SL, Fung MK, Wong FL, Sun HY, Lau KM, Lee ST. Efficient organic photovoltaic devices using a combination of exciton blocking layer and anodic buffer layer. *Journal of Applied Physics* 2006; **100**(9): 094506.
98. Song QL, Li FY, Yang H, Wu HR, Wang XZ, Zhou W, Zhao JM, Ding XM, Huang CH, Hou XY. Small-molecule organic solar cells with improved stability. *Chemical Physics Letters* 2005; **416**(1–3): 42–46.
99. Song QL, Li CM, Wang ML, Sun XY, Hou XY. Role of buffer in organic solar cells using C-60 as an acceptor. *Applied Physics Letters* 2007; **90**(7): 071109.
100. Vogel M, Doka S, Breyer C, Lux-Steiner MC, Fostiropoulos K. On the function of a bathocuproine buffer layer in organic photovoltaic cells. *Applied Physics Letters* 2006; **89**(16): 163501.
101. Halls JJM, Walsh CA, Greenham NC, Marseglia EA, Friend RH, Moratti SC, Holmes AB. Efficient photodiodes from interpenetrating polymer networks. *Nature* 1995; **376**(6540): 498–500.
102. Yu G, Gao J, Hummelen JC, Wudl F, Heeger AJ. Polymer photovoltaic cells—enhanced efficiencies via a network of internal donor-acceptor heterojunctions. *Science* 1995; **270**(5243): 1789–1791.
103. Hiramoto M, Yamaga T, Danno M, Suemori K, Matsumura Y, Yokoyama M. Design of nanostructures for photoelectric conversion using an organic vertical superlattice. *Applied Physics Letters* 2006; **88**(21): 213105.
104. Gebeyehu D, Maennig B, Drechsel J, Leo K, Pfeiffer M. Bulk-heterojunction photovoltaic devices based on donor-acceptor organic small molecule blends. *Solar Energy Materials and Solar Cells* 2003; **79**(1): 81–92.
105. Peumans P, Uchida S, Forrest SR. Efficient bulk heterojunction photovoltaic cells using small-molecular-weight organic thin films. *Nature* 2003; **425**(6954): 158–162.
106. Uchida S, Xue J, Rand BP, Forrest SR. Organic small molecule solar cells with a homogeneously mixed copper phthalocyanine: C60 active layer. *Applied Physics Letters* 2004; **84**(21): 4218–4220.
107. Heutz S, Sullivan P, Sanderson BM, Schultes SM, Jones TS. Influence of molecular architecture and intermixing on the photovoltaic, morphological and spectroscopic properties of CuPc-C60 heterojunctions. *Solar Energy Materials and Solar Cells* 2004; **83**: 229–245.
108. Sullivan P, Heutz S, Schultes SM, Jones TS. Influence of codeposition on the performance of CuPc-C60 heterojunction photovoltaic devices. *Applied Physics Letters* 2004; **84**(7): 1210–1212.
109. Xue J, Rand BP, Uchida S, Forrest SR. Mixed donor-acceptor molecular heterojunctions for photovoltaic applications. II. Device performance. *Journal of Applied Physics* 2005; **98**(12): 124903.
110. Hiramoto M, Fukusumi H, Yokoyama M. Organic solar-cell based on multistep charge separation system. *Applied Physics Letters* 1992; **61**(21): 2580–2582.
111. Opitz A, Bronner M, Bruetting W. Ambipolar charge carrier transport in mixed organic layers of phthalocyanine and fullerene. *Journal of Applied Physics* 2007; **101**: 063709.
112. Yang F, Shtein M, Forrest SR. Controlled growth of a molecular bulk heterojunction photovoltaic cell. *Nature Materials* 2005; **4**(1): 37–41.
113. Shao Y, Sista S, Chu CW, Sievers D, Yang Y. Enhancement of tetracene photovoltaic devices with heat treatment. *Applied Physics Letters* 2007; **90**(10): 103501.
114. Hiramoto M, Suezaki M, Yokoyama M. Effect of thin gold interstitial-layer on the photovoltaic properties of tandem organic solar-cell. *Chemistry Letters* 1990; **3**(3): 327–330.
115. Yakimov A, Forrest SR. High photovoltage multiple-heterojunction organic solar cells incorporating interfacial metallic nanoclusters. *Applied Physics Letters* 2002; **80**(9): 1667–1669.
116. Rand BP, Peumans P, Forrest SR. Long-range absorption enhancement in organic tandem thin-film solar cells containing silver nanoclusters. *Journal of Applied Physics* 2004; **96**(12): 7519–7526.
117. Xue J, Uchida S, Rand BP, Forrest SR. Asymmetric tandem organic photovoltaic cells with hybrid planar-mixed molecular heterojunctions. *Applied Physics Letters* 2004; **85**(23): 5757–5759.
118. Triyana K, Yasuda T, Fujita K, Tsutsui T. Tandem-type organic solar cells by stacking different heterojunction materials. *Thin Solid Films* 2005; **477**(1–2): 198–202.
119. Drechsel J, Maennig B, Kozlowski F, Pfeiffer M, Leo K, Hoppe H. Efficient organic solar cells based on a double p-i-n architecture using doped wide-gap transport layers. *Applied Physics Letters* 2005; **86**(24): 244102.
120. Cheyns D, Gommans H, Odijk M, Poortmans J, Heremans P. Stacked organic solar cells based on pentacene and C-60. *Solar Energy Materials and Solar Cells* 2007; **91**(5): 399–404.
121. Persson NK, Inganas O. Organic tandem solar cells—modeling and predictions. *Solar Energy Materials and Solar Cells* 2006; **90**(20): 3491–3507.

122. Kawano K, Ito N, Nishimori T, Sakai J. Open circuit voltage of stacked bulk heterojunction organic solar cells. *Applied Physics Letters* 2006; **88**(7): 073514.
123. Hadipour A, B. de Boer, Wildeman J, Kooistra FB, Hummelen JC, Turbiez MGR, Wienk MM, Janssen RAJ, Blom PWM. Solution-processed organic tandem solar cells. *Advanced Functional Materials* 2006; **16**(14): 1897–1903.
124. Hanisch J, Ahlswede E, Powalla M. Contacts for semi-transparent organic solar cells. *The European Physical Journal—Applied Physics* 2007; **37**(3): 261–264.
125. Gilot J, Wienk MW, Janssen RAJ. Double and triple junction polymer solar cells processed from solution. *Applied Physics Letters* 2007; **90**: 143512.
126. Dennler G, Prall HJ, Koeppel R, Egginger M, Autengruber R, Sariciftci NS. Enhanced spectral coverage in tandem organic solar cells. *Applied Physics Letters* 2006; **89**(7): 073502.
127. Colsmann A, Junge J, Kayser C, Lemmer U. Organic tandem solar cells comprising polymer and small-molecule subcells. *Applied Physics Letters* 2006; **89**(20): 203506.
128. Durr M, Bamedi A, Yasuda A, Nelles G. Tandem dye-sensitized solar cell for improved power conversion efficiencies. *Applied Physics Letters* 2004; **84**(17): 3397–3399.
129. Coe S, Woo WK, Bawendi M, Bulovic V. Electroluminescence from single monolayers of nanocrystals in molecular organic devices. *Nature* 2002; **420**(6917): 800–803.
130. Rand BP, Xue J, Yang F, Forrest SR. Organic solar cells with sensitivity extending into the near infrared. *Applied Physics Letters* 2005; **87**(23): 233508.
131. Koeppel R, Sariciftci NS, Buchtemann A. Enhancing photon harvesting in organic solar cells with luminescent concentrators. *Applied Physics Letters* 2007; **90**: 181126.
132. Bailey-Salzman RF, Rand BP, Forrest SR. Semitransparent organic photovoltaic cells. *Applied Physics Letters* 2006; **88**(23): 233502.
133. O'Connor B, An KH, Pipe KP, Zhao Y, Shtein M. Enhanced optical field intensity distribution in organic photovoltaic devices using external coatings. *Applied Physics Letters* 2006; **89**(23): 233502.
134. Oyamada T, Sugawara Y, Terao Y, Sasabe H, Adachi C. Top light-harvesting organic solar cell using ultrathin Ag/MgAg layer as anode. *Japanese Journal of Applied Physics Part 1* 2007; **46**(4A): 1734–1735.
135. Brabec CJ. Organic photovoltaics: technology and market. *Solar Energy Materials and Solar Cells* 2004; **83**(2–3): 273–292.
136. Hansel H, Zettl H, Krausch G, Schmitz C, Kisselev R, Thelakkat M, Schmidt HW. Combinatorial study of the long-term stability of organic thin-film solar cells. *Applied Physics Letters* 2002; **81**(11): 2106–2108.
137. Song QL, Wang ML, Obbard EG, Sun XY, Ding XM, Hou XY, Li CM. Degradation of small-molecule organic solar cells. *Applied Physics Letters* 2006; **89**(25): 251118.
138. Potscavage WJ, Yoo S, Domercq B, Kippelen B. Encapsulation of pentacene/C60 organic solar cells with Al2O3 deposited by atomic layer deposition. *Applied Physics Letters* 2007; **90**(25): 253511.
139. Krebs FC, Spanggaard H. Significant improvement of polymer solar cell stability. *Chemistry of Materials* 2005; **17**(21): 5235–5237.
140. Hinsch A, Kroon JM, Kern R, Uhlenndorf I, Holzbock J, Meyer A, Ferber J. Long-term stability of dye-sensitized solar cells. *Progress in Photovoltaics: Research and Applications* 2001; **9**(6): 425–438.
141. Wang P, Zakeeruddin SM, Moser JE, Humphry-Baker R, Comte P, Aranyos V, Hagfeldt A, Nazeeruddin MK, Gratzel M. Stable new sensitizer with improved light harvesting for nanocrystalline dye-sensitized solar cells. *Advanced Materials* 2004; **16**(20): 1806–1811.
142. Kroon JM, Bakker NJ, Smit HJP, Liska P, Thampi KR, Wang P, Zakeeruddin SM, Gratzel M, Hinsch A, Hore S, Wurfel U, Sastrawan R, Durrant JR, Palomares E, Pettersson H, Gruszecki T, Walter J, Skupien K, Tulloch GE. Nanocrystalline dye-sensitized solar cells having maximum performance. *Progress in Photovoltaics: Research and Applications* 2007; **15**(1): 1–18.
143. Kwong RC, Nugent MR, Michalski L, Ngo T, Rajan K, Tung YJ, Weaver MS, Zhou TX, Hack M, Thompson ME, Forrest SR, Brown JJ. High operational stability of electrophosphorescent devices. *Applied Physics Letters* 2002; **81**(1): 162–164.